Journal of Fluorescence, Vol. 9, No. 1, 1999

New Perspectives of Fluorescence Correlation Spectroscopy

Antonie J. W. G. Visser[1,2] and Mark A. Hink[1]

Received October 19, 1998; accepted October 27, 1998

The principle of fluorescence correlation spectroscopy is outlined. The technique has been applied to a mutant of the well-known green fluorescent protein. A comparative study has been made with time-resolved fluorescence anisotropy. The latter experiment shows that the fluorophore is rigidly bound inside the protein matrix follows the rotation of the whole protein and does not show any fast restricted motion. It is evident from fluorescence correlation spectroscopy that some excited-state reaction plays a role, since the autocorrelation traces show a significant effect on the incident laser power. Other potential applications of fluorescence correlation spectroscopy are presented as taken from very recent publications.

KEY WORDS: Fluorescence correlation; fluorescence anisotropy; green fluorescent protein; single molecule detection.

INTRODUCTION

Fluorescence correlation spectroscopy (FCS) is a sensitive technique developed for studying dynamic processes of fluorescently marked molecules under equilibrium conditions. FCS measures fluctuations of fluorescence intensity in an open volume element created by a focused laser beam. Any dynamic process that is accompanied by a fluorescence change can be measured. The fluorescence intensity fluctuations can be caused either by diffusion of fluorescently labeled molecules in- and out of the light cavity, by chemical reaction kinetics such as arising from association and dissociation of a molecular complex, by conformational transitions in macromolecules, or by flow of fluorescent molecules. Fast correlation of the intensity fluctuations is then used to evaluate the particle number (concentration), reaction dynamics, and diffusion rates. The concepts for FCS date back to the early 1970s [1–5]. It is due to recent developments in confocal microscopy (leading to significant fluorescent background suppression), efficient photon detection and correlation, that the measurements can now be performed rapidly [6–12].

Briefly, the principle of FCS is as follows. A small open-volume element is created by a focused laser beam. In this confocal volume fluorescent molecules will be excited, leading to a burst of fluorescence photons. Owing to Brownian motion, molecules will enter or leave the excitation cavity, which results in changes in the detected fluorescence intensity. These intensity fluctuations can be rapidly measured with a fast photon detector and autocorrelated on-line. The autocorrelation function provides information on diffusion properties of fluorescent molecules. Small-sized molecules move more rapidly through the confocal volume element than large macromolecules. This is the basis of the advantage of the technique: one can measure molecular interactions at the unsurpassed sensitivity of single-molecule detection. When a small, fluorescent ligand interacts with a large macromolecule, it can be immediately determined by a retarded diffusion and the interaction can be fully quantified. Not only transport properties but also chemical reactions like association-dissociation kinetics [13,14] and photochemical reactions such as triplet-state kinetics can be investigated

[1] MicroSpectroscopy Center, Department of Biomolecular Sciences, Laboratory of Biochemistry, Wageningen Agricultural University, Dreijenlaan 3, 6703 HA Wageningen, The Netherlands.
[2] To whom correspondence should be addressed.

1053-0509/99/0300-0081$16.00/0

with the technique [15]. A schematic view of the concepts and causes of FCS has been presented in Fig. 1.

The diffusion constant for translational movement can be determined from the normalized autocorrelation function $G(\tau)$, which relates the fluorescence intensity I at a time t to that τ seconds later:

$$G(\tau) = \frac{\langle I(t) \cdot I(t+\tau)\rangle}{\langle I\rangle^2} = \frac{\langle I\rangle^2 + \langle \delta I(t) \cdot \delta I(t+\tau)\rangle}{\langle I\rangle^2} \tag{1}$$

Here δI denotes the fluctuation of the fluorescence intensity around the mean value $\langle I\rangle$. The detected fluorescence intensity is dependent on the concentration and spectroscopic properties of the fluorescent probe and the detection efficiency of the experimental setup. Assuming a detection volume, which is Gaussian shaped in three dimensions [16], the autocorrelation function can be written as

$$G(\tau) = 1 + \left[(1 - F + F \cdot e^{-\lambda\tau})/N_m \left(1 + \frac{4D_{tran}}{\omega_1^2 \cdot \tau}\right) \times \left(1 + \frac{4D_{tran}}{\omega_2^2 \cdot \tau}\right)^{1/2}\right] \tag{2}$$

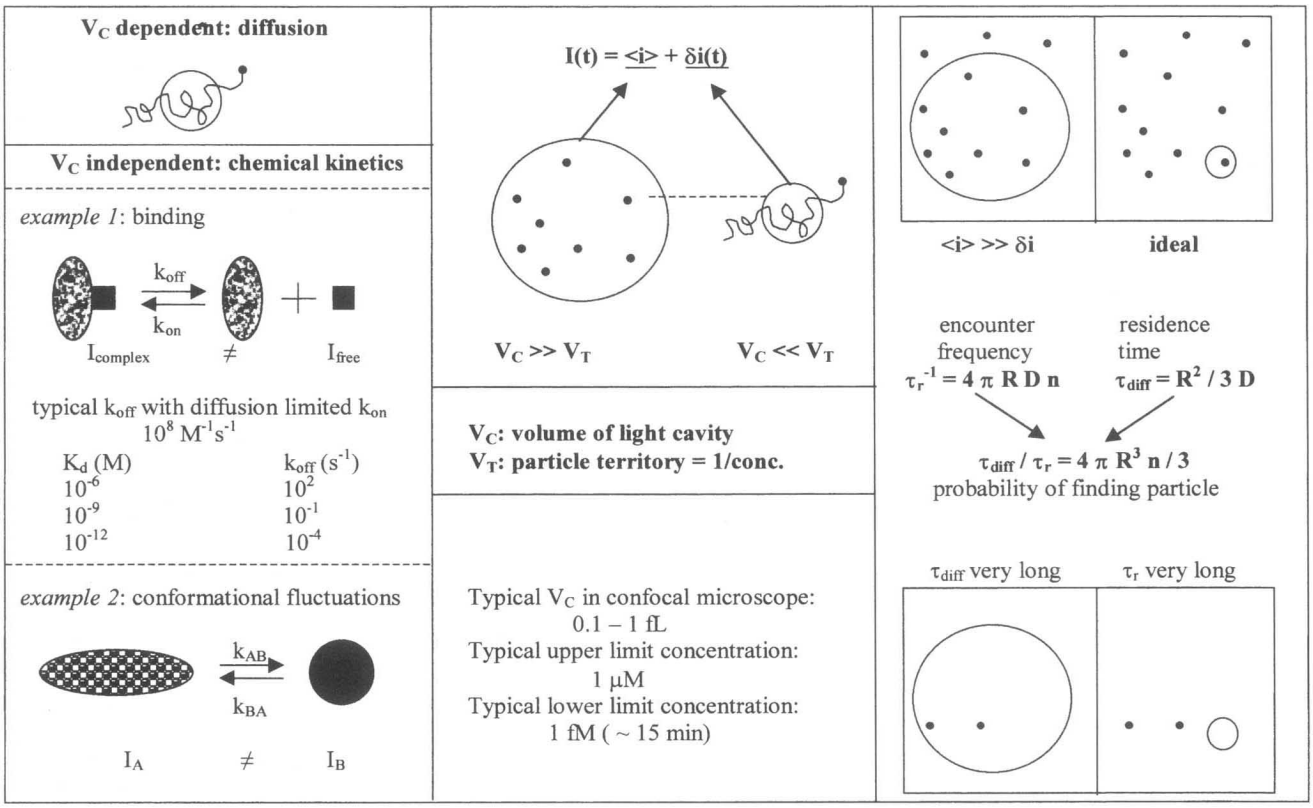

Fig. 1. Causes and concepts of fluorescence intensity fluctuations. The first cause is connected with transport of single molecules in and out of the laser cavity. This diffusion phenomenon will depend on the volume of the light cavity V_c. The larger the volume, the longer the fluorescent molecule resides therein, resulting in longer diffusion times. On the other hand, FCS events related to chemical relaxation such as the dissociation rate of a protein-bound ligand or conformational transitions in a single protein molecule are not dependent on the size of the cavity volume, since these phenomena take place in the still smaller molecular territory (V_T). Chemical relaxation can be measured only when the fluorescence efficiencies of the molecules involved are different. In principle the off-rate constant (k_{off}) of a binding equilibrium reaction can be determined during the residence time in the volume element (example 1, left). Alternatively, the interconversion rate between two macromolecular conformations can be determined (example 2, left). The cross sections of the confocal volume element depicted in the center account for the relative volumes of the light cavity V_c and of the particle territory V_T, which determine whether we have large average fluorescence intensities ($V_c \gg V_T$) or large fluctuations ($V_c \ll V_T$). The particle territory is the reciprocal of the concentration. The right side gives a kinetic picture. Kinetically there are two characteristic times to consider: the reciprocal of the encounter frequency τ_r^{-1} of the particle to enter the light cavity of radius R and the residence time of the particle in the cavity τ_{diff}. D is the translation diffusion coefficient and n is the particle density (number of particles/cm^3). The ratio τ_{diff}/τ_r is simply the ratio of volumes of light cavity and particle territory and reflects the probability of finding a particle inside the cavity (further details can be found in Ref. 9).

where D_{tran} denotes the translational diffusion constant, N_m the number of fluorescent particles in the detection volume, and both ω_1 and ω_2 are constants corresponding to the radial and axial radii (e^{-2} point of the Gaussian beam) of the sampling volume element. Equation (2) also contains a term F, describing the fraction of molecules in the triplet state and the characteristic triplet decay rate λ. The translational diffusion constant is related to the diffusion time τ_{diff} via

$$D_{tran} = \frac{\omega_1^2}{4 \cdot \tau_{diff}} \tag{3}$$

where τ_{diff} is the time needed to diffuse over a distance ω_1. The square of the laser beam waist ω_1 can be obtained by calibration with a rhodamine 6G solution having a known diffusion constant of $2.8 \cdot 10^{-10}$ m^2 s^{-1} at 20°C. The hydrodynamic radius of the fluorescent particle, r_h, is defined by Eq. (4) as

$$r_h = \frac{k \cdot T}{6 \cdot \pi \cdot D_{tran} \cdot \eta} \tag{4}$$

where k is the Boltzmann constant, T the temperature, and η the viscosity.

In this contribution we would like to illustrate the potential of FCS applied to the well-known green fluorescent protein (GFP) from the jellyfish *Aequorea victoria*, which has received widespread utilization as a natural fluorescent marker for gene expression and localization of gene products (see Refs. 17 and 18 for recent reviews). First, we show that a combination of FCS and time-resolved fluorescence anisotropy (TRFA) will lead to very specific complementary information on the motional dynamics of this protein. TRFA will yield information on both overall rotation and internal restricted motion of the protein. Second, the chromophore in GFP undergoes some peculiar excited-state processes upon an increase in the laser power in the FCS experiment. Finally, some interesting FCS applications have appeared in the very recent literature, suggesting that the method has left the pioneering stage and can now be applied to widely different research areas.

EXPERIMENTAL

Details of the preparation of GFP will be given elsewhere (Hink *et al.*, manuscript submitted). To change the fluorescence excitation peak of wild-type green fluorescent protein from 396 to 488 nm, two amino acid mutational changes were introduced: Phe64 was replaced by Leu and Ser65 by Thr. The protein was dissolved in 0.1 *M* Tris–HCl buffer, pH 7.5. Concentrations were ca. 1–5 n*M* for FCS experiments and ca. 100 n*M* for steady-state fluorescence spectral and time-resolved fluorescence experiments. All experiments were conducted at 20–22°C.

Full details concerning the FCS experimental setup and data analysis as currently used by our research group can be found in Ref. 19. The 488-nm Ar ion laser line was used for excitation and the "fluorescein" filter set selected the emission wavelength range. The laser power was measured using a power meter, which was mounted in one of the objective holders in the revolver. Then it was assumed that the transmission efficiency of the Zeiss Apochromat 40 × 1.2 objective lens is ca. 85%. To determine the power per area, the focal spot dimension was calculated from $\pi\omega_1^2$ and amounted to 2.45 10^{-13} m^2. In this way the power densities listed in Table I are determined, for instance, when no neutral density (ND) filter is used, the power/area = 5.13 10^9 W m^{-2}.

Time-resolved polarized fluorescence experiments were carried out using a picosecond laser system and time-correlated single-photon counting as described in detail elsewhere [20]. The excitation wavelength was 480 nm and the fluorescence was selected by using a bandpass filter transmitting between 500 and 550 nm. The excitation and emission spectra were obtained with a Spex Fluorolog 3–22 spectrofluorometer.

RESULTS AND DISCUSSION

Fluorescence Properties of the GFP Mutant

In Fig. 2 all experiments on the GFP variant with enhanced blue–green light absorption are summarized. The fluorescence excitation and emission spectra are given in the top panel. Without converting the spectra into wavenumber scale, it can already be seen that the emission and excitation spectra do not exhibit a mirror image relationship. The excitation spectrum is much broader than the fluorescence spectrum (this effect would be even more pronounced when the spectra are presented on a wavenumber scale). The conclusion is that the absorption spectrum between 450 and 510 nm contains at least two overlapping electronic transitions.

An example of experimental and fitted fluorescence decay curves is presented in the middle panel in Fig. 2. The curves are drawn in a semilogarithmic fashion to illustrate that the decay is clearly heterogeneous. Three fluorescence lifetimes were needed to give an optimal fit. The main fluorescence lifetime is 2.6 ns, but lifetimes of 0.50 and 4.9 ns are also present. The heterogeneity of

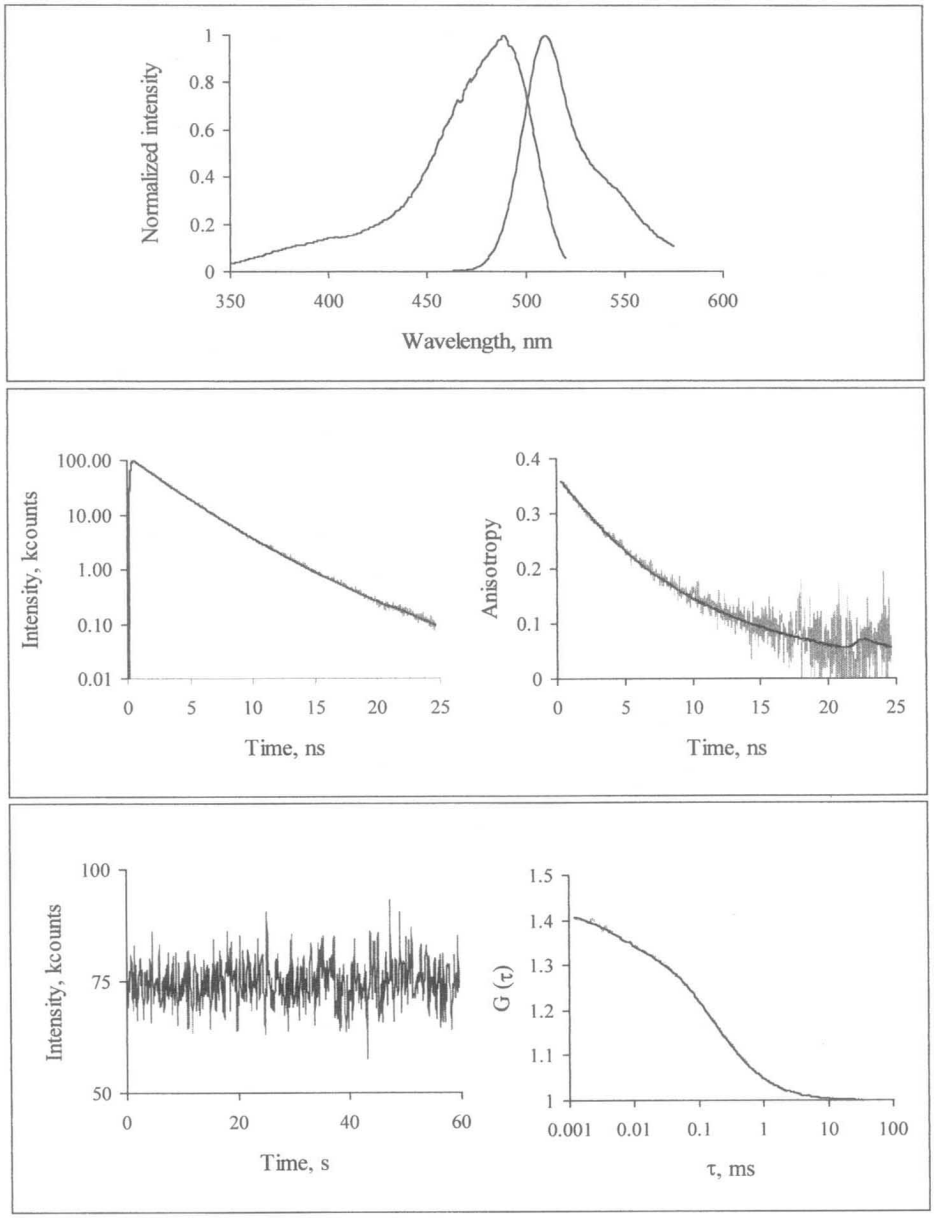

Fig. 2. Fluorescence properties of the GFP mutant with enhanced blue–green light absorption. The top panel shows the corrected, normalized excitation (λ_{em} = 510 nm) and emission spectra (λ_{exc} = 450 nm). The center panel accounts for the experimental and fitted fluorescence decay curves and anisotropy decay curves. The bottom panel gives an example of a FCS experiment with the shower of emission photons (left) and the experimental and fitted autocorrelation curves (right). Numerical results and further details are given in the text.

the fluorescence decay is consistent with the reaction scheme proposed previously from subpicosecond time-resolved fluorescence spectroscopy [21,22]. This scheme has taken into account equilibria between different ground and excited states, proton transfer, and photoconversion processes. These multiple states and the interconversion between them would lead to an inherent nonexponential decay as observed. An example of the experimental and fitted fluorescence anisotropy decay curves is given in the center panel in Fig. 2. The decay analysis yields a single rotational correlation time ϕ of 11 ns. The fluorophore is rigidly bound in the protein matrix and rotates

together with the whole protein, since no shorter decay component is visible in the anisotropy decay. This observation is in full agreement with the three-dimensional structures in which the fluorophore is rigidly incorporated in the central helix [23–25].

The GFP mutant has excellent properties for FCS. In the bottom panel in Fig. 2 a representative example of a "single-molecule" FCS experiment is given. In the lower left panel the shower of fluorescence photons during 60 s is depicted. In the lower right panel the autocorrelation curves (experimental and fitted) are presented. The diffusion time (τ_{diff} = 168 μs) is in very good agreement with what is expected for a protein of 27-kDa mass. The concentration is accurately determined (4.5 n*M*), because in this experiment both the number of particles (2.8) and the probe volume (1.0 fL) are known. The figure of merit in FCS is a sufficient number of photon counts that a single molecule can emit during its residence in the sampling volume. The GFP fluorophore with its 30-kHz fluorescence photons detected per molecule nicely fulfills these conditions, provided that the excitation laser power is kept relatively low (*vide infra*).

Excitation Intensity Dependence of Autocorrelation Traces of the GFP Mutant

In FCS experiments we found that the autocorrelation traces of the used GFP strongly depends on the incident laser power. This observation is illustrated in Fig. 3 (top panel), in which several autocorrelation curves taken with different laser excitation intensities have been overlayed. When the data were analyzed, the apparent τ_{diff} turned out to shorten with increasing laser power, even to a point where the apparent τ_{diff} is of the same order as the diffusion time of the rhodamine 6G standard (Fig. 3, lower panel, and Table I). It is very likely that this anomaly must be ascribed to the existence of a dark state, which is populated at a relatively high laser power, similarly as for the triplet state in the singlet–triplet cycle [15]. The data analysis, however, shows that the triplet yield of the GFP mutant is not affected at all by a variation of laser power (Table I). Therefore, the results suggest that another mechanism is operative. Apparently, a high laser power brings the GFP mutant in a kind of dark state, from which it is not converted to the ground state responsible for emission after photoexcitation. This interpretation is in agreement with the reaction scheme derived from the ultrarapid fluorescence kinetics [21,22] and from the blinking behavior as observed from single-molecule fluorescence detection of GFP in a polyacrylamide gel [26]. Further research is needed to corroborate this point.

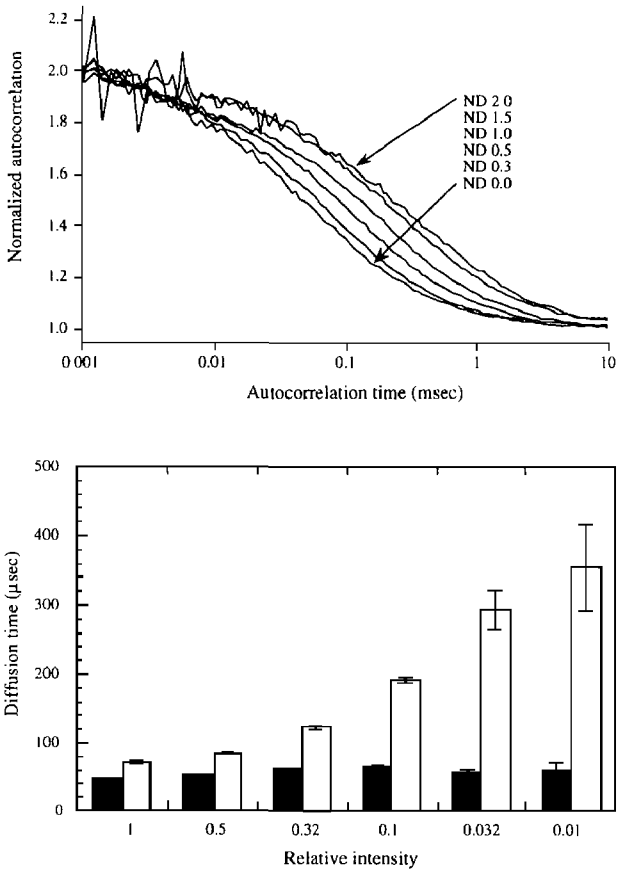

Fig. 3. Normalized, experimental autocorrelation traces of the GFP mutant with enhanced blue–green light absorption taken with increasing laser power (top panel). Neutral density (ND) filters are used to decrease incident laser power (for instance, ND = 1 means that the laser power has been diminished by a factor of 10). The lower panel shows the apparent diffusion times of the GFP mutant (open bars) as a function of the relative intensity of the incident laser beam. For comparison, the results of the standard compound rhodamine 6G are presented as well (fill bars) to show that this compound gives approximately the same diffusion time. The error bars are obtained from at least 15 experiments.

New Developments in FCS

Interesting FCS applications have appeared in the very recent literature. A study on the kinetics of conformational fluctuations in DNA hairpin loops is described in Ref. 27. The authors have investigated the opening and closing of the loop by using a so-called DNA molecular beacon, which consists of a fluorescent probe at one end and a quencher attached to the other end of the loop. The correlation function of the beacon (G_{beacon}) contains contributions of both diffusion and chemical kinetics. As a control sample a DNA hairpin without quencher is used, for which the correlation function ($G_{control}$) consists of diffusion only. The ratio $G_{beacon}(t)/G_{control}(t)$ isolates the kinetics part yielding the chemical reaction rate $1/\tau_{reaction} = k_- + k_+$, where k_- is the opening and k_+ the closing

Table I. Results of Analysis of Autocorrelation Curves of Mutant GFP as Function of Laser Excitation Power[a]

τ_{diff} (μs)	N	τ_{trip} (μs)	% triplet	cpm (kHz)	Power/area [(W/m^2)*10^9]
72 ± 2	10.2 ± 0.4	4.8	21 ± 1	15.0 ± 0.5	6.23
86 ± 1	6.5 ± 0.3	4.0	18 ± 1	23.0 ± 0.4	3.08
124 ± 3	4.2 ± 0.1	3.5	18 ± 1	31.0 ± 0.4	1.50
192 ± 5	3.5 ± 0.1	5.0	17 ± 1	29.0 ± 0.3	0.62
294 ± 29	3.4 ± 0.1	14	17 ± 3	14.0 ± 0.4	0.18
355 ± 62	3.3 ± 0.2	24	17 ± 3	5.4 ± 0.4	0.06

[a] The standard errors are based on 15 determinations. τ_{diff}, diffusion time; N, number of particles in the sampling volume element; τ_{trip}, triplet-state lifetime; % triplet, the fraction of molecules in the triplet state [F in Eq. (2)]; cpm, number of photon counts emitted per molecule. Laser power is estimated as described under Experimental.

rate constant of the loop. Another experiment gave the equilibrium constant $K = k_-/k_+$ so that both rate constants can be determined separately.

An investigation on conformational fluctuations in single DNA molecules is given in Ref. 28. The authors used a fluorescent probe linked to the forward primer of a 217-bp DNA oligonucleotide and a biotin molecule linked to the reversed primer. The DNA derivative is then attached to a coverslip containing streptavidin. The conformational fluctuations are monitored via FCS and the autocorrelation curves are analyzed via a stretched exponential model ($A\exp(-k_{reaction}t)^{\beta}$, $k_{reaction}$ is the sum of reaction rates in each direction, similarly as in the hairpin loop experiment [27], and β is the so-called stretch parameter), which indicates the presence of a distribution of transition rates between two conformations. These experiments show that it is possible to obtain information on the properties of a single DNA molecule as distinguished from the collective properties of a whole ensemble of DNA molecules. One of the key questions is, then, Do all DNA molecules have the same reaction rate ($k_{reaction}$) or do DNA molecules contribute individually to yield a narrow distribution of rates? A general formulation of this principle has been given by Wang and Wolynes [29]. Properties found for the molecular ensemble can also be a property of a single molecule (the homogeneous case). Alternatively, the ensemble behavior can be represented as a collection of individual molecules each having slightly different properties (the inhomogenous case). In the latter case the principle of ergodicity will be important. Individual DNA molecules will experience different reaction rates, but provided that enough time is given, the time average of the reaction rate of each single DNA molecule will be identical to the ensemble average collected from many DNA molecules.

Dual-color fluorescence cross-correlation spectroscopy is a new approach to probe interactions between (macro-)molecules that carry different fluorescent labels [30]. Dual-color fluorescence cross-correlation spectroscopy probes molecules that simultaneously emit fluorescence at two distinct wavelengths. Real-time enzyme kinetics and rapid enzymatic assay processing for high-throughput screening with the aid of dual-color fluorescence cross-correlation spectroscopy are described, respectively, in Refs. 31 and 32.

The next challenging step is to apply the technique to living cells [11,33]. We shall call the technique fluorescence correlation microscopy (FCM) when it is applied to cellular systems. Preliminary FCM experiments carried out by us on living cells indicated that some technical problems have to be solved before the methodology can be routinely applied. Cellular autofluorescence and photobleaching of the fluorescent probe are important perturbing factors which should be eliminated before FCM is feasible. Dual-color fluorescence cross-correlation spectroscopy may be very helpful in suppressing the uncorrelated autofluorescence in cells. Furthermore, in order to study cellular systems in real time, rapid scanning through the cell in three dimensions combined with efficient data collection needs systematic investigation [34–37]. The occurrence of fluorescence resonance energy transfer (FRET; operating in the 2- to 5-nm distance range) between two juxtaposed fluorescent molecules can be perfectly measured using the concept of dual-color fluorescence cross-correlation spectroscopy, where one single laser wavelength excites the donor and two detection channels isolate the emissions of donor and acceptor. This FRET approach allows the observation of interacting molecules in a cellular environment and provides us with nanometer resolution in confocal microscopy.

ACKNOWLEDGMENTS

We are grateful to Arjen Schots for making the GFP mutant available, to Jan-Willem Borst and Arie van Hoek

for assistance with the collection of spectral and time-resolved flourescence data of GFP, and to Nina Visser for preparation of the figures. This work was supported by grants from the Council of Earth and Life Sciences of The Netherlands Organization of Scientific Research (NWO).

REFERENCES

1. E. L. Elson and D. Magde (1974) *Biopolymers* **13**, 1–27.
2. D. Magde, E. L. Elson, and W. W. Webb (1974) *Biopolymers* **13**, 29–61.
3. M. Ehrenberg and R. Rigler (1974) *Chem. Phys.* **4**, 390–401.
4. S. R. Aragon and R. Pecora (1975) *Biopolymers* **14**, 119–138.
5. D. Magde, W. W. Webb, and E. Elson (1978) *Biopolymers* **17**, 361–376.
6. N. L. Thompson (1991) in J. R. Lakowicz (Ed.), *Topics in Fluorescence Spectroscopy, Vol. 1*, Plenum Press, New York, pp. 337–378.
7. R. Rigler, J. Widengren, and Ü. Mets (1993) in O. S. Wolfbeis (Ed.), *Fluorescence Spectroscopy*, Springer Verlag, Berlin, pp. 13–24.
8. R. Rigler, Ü. Mets, J. Widengren, and P. Kask (1993) *Eur. Biophys. J.* **22**, 169–175.
9. M. Eigen and R. Rigler (1994) *Proc. Natl. Acad. Sci. USA* **91**, 5740–5747.
10. P. I. H. Bastiaens, E. H. W. Pap, J. Widengren, R. Rigler, and A. J. W. G. Visser (1994) *J. Fluoresc.* **4**, 377–384.
11. K. M. Berland, P. T. C. So, and E. Gratton (1995) *Biophys. J.* **68**, 694–701.
12. S. Maiti, U. Haupts, and W. W. Webb (1997) *Proc. Natl. Acad. Sci. USA* **94**, 11753–11757.
13. M. Kinjo and R. Rigler (1995) *Nucleic Acids Res.* **23**, 1795–1799.
14. B. Rauer, E. Neumann, J. Widengren, and R. Rigler (1996) *Biophys. Chem.* **58**, 3–12.
15. J. Widengren, Ü. Mets, and R. Rigler (1995) *J. Phys. Chem.* **99**, 13368–13379.
16. S. R. Aragon and R. Pecora (1976) *J. Chem. Phys.* **64**, 1791–1803.
17. S. M. Leffel, S. A. Mabon, and C. N. Stewart Jr. (1997) *BioTechniques* **23**, 912–917.
18. R. Y. Tsien (1998) *Ann. Rev. Biochem.* **67**, 509–544.
19. M. Hink and A. J. W. G. Visser (1998) in W. Rettig, B. Strehmel, and S. Schrader (Eds.), *Applied Fluorescence in Chemistry, Biology and Medicine*, Springer-Verlag, Berlin, pp. 101–118.
20. A. van Hoek and A. J. W. G. Visser (1992) *Proc. SPIE* **1640**, 325–329.
21. M. Chattoraj, B. A. King, G. U. Bublitz, and S. G. Boxer (1996) *Proc. Natl. Acad. Sci. USA* **93**, 8362–8367.
22. H. Lossau, A. Kummer, R. Heinecke, F. Pöllinger-Dammer, C. Kompa, G. Bieser, T. Jonsson, C. M. Silva, M. M. Yang, D. C. Youvan, and M. E. Michel-Beyerle (1996) *Chem. Phys.* **213**, 1–16.
23. M. Ormö, A. B. Cubitt, K. Kallio, L. A. Gross, R. Y. Tsien, and S. J. Remington (1996) *Science* **273**, 1392–1395.
24. F. Yang, L. G. Moss, and G. N. Phillips (1996) *Nature Biotechnol.* **14**, 1246–1251.
25. K. Brejc, T. K. Sixma, P. A. Kitts, S. R. Kain, R. Y. Tsien, M. Ormö, and S. J. Remington (1997) *Proc. Natl. Acad. Sci. USA* **94**, 2306–2311.
26. R. M. Dickson, A. B. Cubitt, R. Y. Tsien, and W. E. Moerner (1997) *Nature* **388**, 355–358.
27. G. Bonnet, O. Krichevsky, and A. Libchaber (1998) *Proc. Natl. Acad. Sci. USA* **95**, 8602–8606.
28. S. Wennmalm, L. Edman, and R. Rigler (1997) *Proc. Natl. Acad. Sci. USA* **94**, 10641–10646.
29. J. Wang and P. Wolynes (1995) *Phys. Rev. Lett.* **74**, 4317–4320.
30. P. Schwille, F.-J. Meyer-Almes, and R. Rigler (1997) *Biophys. J.* **72**, 1878–1886.
31. U. Kettling, A. Koltermann, P. Schwille, and M. Eigen (1998) *Proc. Natl. Acad. Sci. USA* **95**, 1416–1420.
32. A. Koltermann, U. Kettling, J. Bieschke, T. Winkler, and M. Eigen (1998) *Proc. Natl. Acad. Sci. USA* **95**, 1421–1426.
33. J. C. Politz, E. S. Brown, D. E. Wolf, and T. Pederson (1998) *Proc. Natl. Acad. Sci. USA* **95**, 6043–6048.
34. N. O. Petersen, P. L. Hoddelius, P. W. Wiseman, O. Seger, and K.-E. Magnusson (1993) *Biophys. J.* **65**, 1135–1146.
35. D. E. Koppel, F. Morgan, A. E. Cowan, and J. H. Carson (1994) *Biophys J.* **66**, 502–507.
36. K. M. Berland, P. T. C. So, Y. Chen, W. W. Mantulin, and E. Gratton (1996) *Biophys. J.* **71**, 410–420.
37. Z. Huang and N. L. Thompson (1996) *Biophys. J.* **70**, 2001–2007.